Study of the dc and ac electrical properties of an yttria-stabilized zirconia single crystal $[(ZrO_2)_{0.88}$-$(Y_2O_3)_{0.12}]$

P. Abelard

Centre de Recherches sur la Physique des Hautes Températures, Centre National de la Recherche Scientifique, 45045 Orléans-Cedex, France and Laboratoire de Minéralogie, Université d'Orléans, 45046 Orléans-Cedex, France

J. F. Baumard

Centre de Recherches sur la Physique des Hautes Températures, Centre National de la Recherche Scientifique, 45045 Orléans-Cedex, France

(Received 15 December 1981)

The electrical properties of single crystals of yttria-stabilized zirconia $[(ZrO_2)_{0.88}$-$(Y_2O_3)_{0.12}]$, known to be an essentially anionic conductor, are studied in wide ranges of temperature (400—1100 K) and frequency (1.6 Hz—100 kHz). The dc electrical conductivity is temperature activated, and the activation energy changes continuously from 1.17 to 1.33 eV when going from low to high temperatures. The ac electrical conductivity is an increasing function of frequency. It obeys a power-law dependence $\sigma(\omega) \propto \omega^n$ with different exponents below ($n = 0.85$) and above ($n = 0.64$) a transition frequency ω_T. In the measurable frequency range, the latter is temperature activated as the electrical conductivity. The observed frequency dispersion is attributed to interactions between mobile oxygen vacancies and randomly distributed frozen-in yttrium dopant ions and is analyzed with the help of the continuous-time random-walk theory developed by Scher and Lax.

I. INTRODUCTION

Pure zirconia oxide ZrO_2 is known to possess the cubic fluorite structure only at very high temperatures, above about 2600 K. However, the cubic form can be stabilized at lower temperatures through the formation of solid solutions with CaO, Y_2O_3, or some rare-earth oxides.[1] Oxygen vacancies form to preserve local charge balance. These defects are known to be very mobile and responsible for the high ionic conductivity of these materials.[1] These compounds have already found numerous applications such as oxygen sensing systems.[2]

Numerous dc or low-frequency ac electrical conductivity measurements have established that the ionic conductivity is not proportional to the dopant concentration as expected from simple transport theory.[3] In the single-phase region, a decrease in the electrical conductivity and simultaneously an increase in the activation energy are observed when increasing dopant content, a very interesting fact that has received several theoretical interpretations.[4,5] As pointed out by Bauerle[6] in a study of stabilized zirconia, ac electrical measurements and complex admittance representation allow the separation of several contributions to the total cell impedance, arising from bulk conduction and interfacial phenomena, as polarization effects at the electrode-electrolyte interfaces, whenever the related time constants for the individual processes are different enough. However, a detailed study of the electric and dielectric bulk properties as a function of frequency has never been done and is the aim of this paper. Experimental data are presented and a microscopic interpretation, based upon the theory of stochastic transport in disordered systems, developed by Scher and Lax,[7] is given.

II. EXPERIMENTAL PROCEDURE

The specimens used in this investigation were $[(ZrO_2)_{0.88}$-$(Y_2O_3)_{0.12}]$ single crystals grown by a Czochralski technique, using a rf furnace and a cold container,[8] kindly supplied by Dr. Tatarintsev. The dopant concentration was ascertained by x-ray microprobe analysis. The lattice parameter a, equal to 5.145 Å, was measured with a conventional x-ray diffraction technique using germanium powder as a standard. Several disks with different thicknesses, approximately 8 mm in diameter, were cut in the same boule. The two faces were coated with gold, platinum, or silver paste. Very little

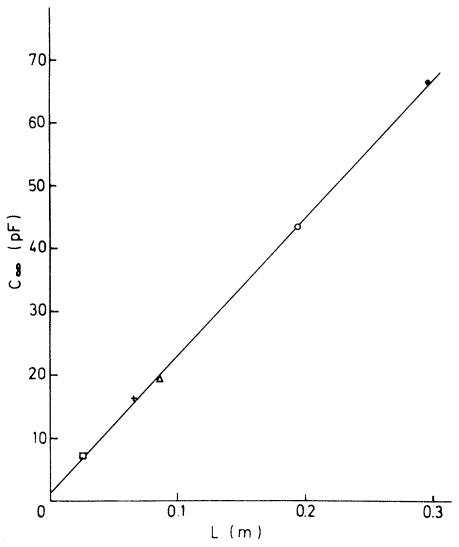

FIG. 1. Plot of capacity C_∞ at 100 kHz and room temperature for several samples, identified with the following symbols: □, +, △, ○, ● as a function of the geometrical factor $L = A/W$.

electrode effects were observed with the latter which was extensively used.

The electrical measurements were performed in an arrangement that allows the separation of the real and imaginary parts of the sample impedance. A variable frequency alternating voltage (1.6 Hz—100 kHz) is applied to the cell assembly in series with a standard resistor. The voltage developed across the resistor is analyzed with the help of a double lock-in amplifier giving the in-phase and out-of-phase components of the current with respect to the emf from the frequency generator. It is then straightforward to calculate the real and imaginary parts of the admittance or impedance of the cell assembly. The cell was introduced into a furnace, where the temperature was maintained constant within 0.25 K during the measurements and varied over the range 400—1100 K.

The experimental setup was tested in the vicinity of room temperature and at 100 kHz by inserting samples of various thicknesses. Under these conditions, the sample is equivalent to a pure capacitor. In Fig. 1, a plot of the capacity C_∞ versus geometrical factor $L = A/W$, where A is the electrode area and W the sample thickness, suggests that a small additional capacity, about 1.5 pF in magnitude, arises from the leads and/or the electronic equipment. The slope of the observed straight line is directly related to the high-frequency dielectric constant of the material ϵ_∞ according to the relation $C_\infty = \epsilon_0 \epsilon_\infty L$, where ϵ_0 is the free-vacuum permittivity. The deduced value of 25 ± 1 is in fair agreement with that calculated from the constant level of infrared reflectivity, 25.7.[9] This means that few, if any, relaxation processes in the mi-

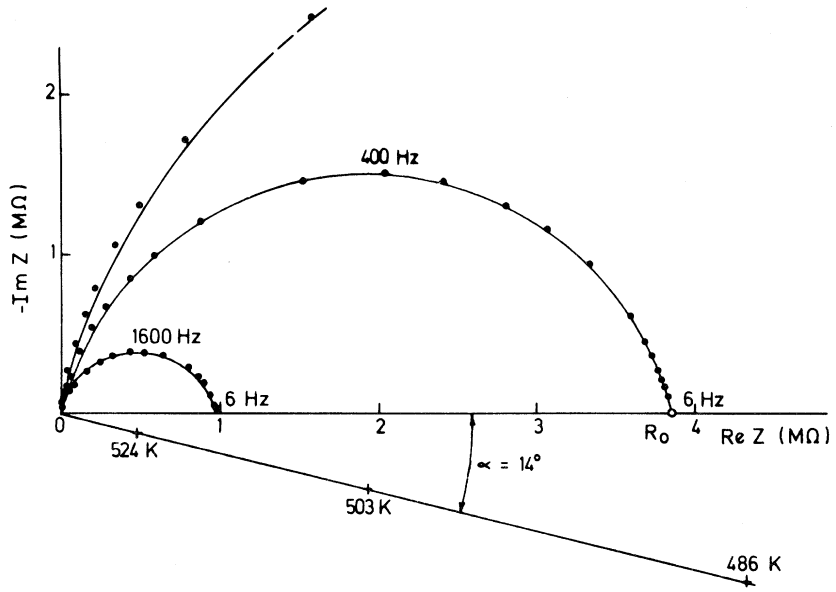

FIG. 2. In the complex impedance representation (ReZ-ImZ), at a given temperature, experimental data points are distributed along part of a circle. Intersection of the circle with the real axis allows the dc resistance R_0 of the sample to be determined at the temperature in question. Three temperatures have been considered (486, 503, and 524 K). Corresponding circles, the centers of which are identified with crosses, are depressed below the real axis by the same angle $\alpha = 14°$.

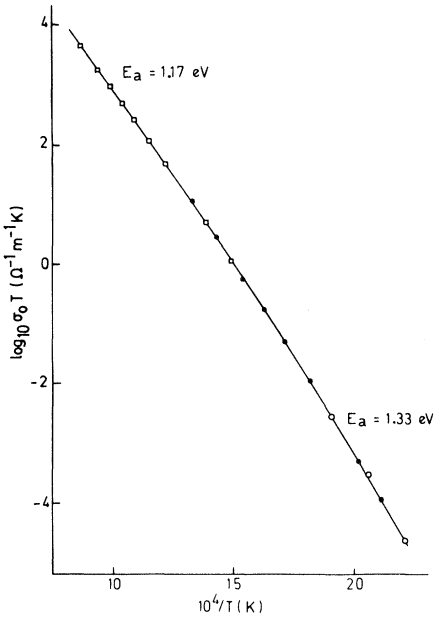

FIG. 3. Plot of the dc electrical conductivity as a function of the temperature in the usual $\log_{10}(\sigma_0 T)$ vs $1/T$ system of coordinates (same symbols as in Fig. 1). Slope of the curve gives the effective activation energy at the temperature considered.

crowave and/or infrared range contribute significantly to the dielectric function itself.

III. COMPLEX IMPEDANCE REPRESENTATION

Conductivity in yttria-stabilized zirconia is known to be essentially anionic over a wide temperature range. As a consequence, under application of an electric field, electrode polarization is likely to occur in addition to transport effects in the bulk. The original work of Bauerle has shown that each individual contribution to the cell impedance becomes apparent in the so-called admittance representation (ReY-ImY). In the following, for reason of convenience, the complex impedance representation (ReZ-ImZ) was preferred. However, the two curves in both planes are simply related through a geometrical inversion, e.g., via $Y=1/Z$.

In agreement with the results of previous studies,[6,10] our experimental data points, in the frequency range investigated and at moderate temperatures, lie along parts of circles passing through the origin, the centers of which are depressed below the real axis by a small angle $\alpha=14°$ (see Fig. 2). When temperature is raised, a second circle becomes increasingly important which, contrarily to the first one, is sensitive to the nature of electrodes and to the oxygen partial pressure in the surrounding atmosphere. It may be attributed to interface phenomena[11] between the electrolyte itself, the metallic electrodes and the gaseous phase. It was minimized by the use of silver electrodes and its study lies outside the scope of this paper.

As shown by the proportionality to the geometrical factor L, the intersection of the first circle with the real axis gives the dc bulk resistance R_0 of the sample. In Fig. 3 $\log_{10}(\sigma_0 T)$ is plotted versus $1/T$, where σ_0 is the bulk electrical conductivity of the material and T the absolute temperature. The conductivity is thermally activated and a gradual change of the activation energy from 1.17 to 1.33 eV is observed from high to low temperature. Such a behavior is in agreement with published literature data.[1,10] For instance, Schouler *et al.*[10] reported values of 0.86 and 1.10 eV, respectively, in their study of a single crystal with a lower yttria content $[(ZrO_2)_{0.91}$-$(Y_2O_3)_{0.09}]$. Increasing the dopant content is known experimentally to result in a higher activation energy for the transport process and finally to lower the electrical conductivity.[4]

IV. ac ELECTRICAL CONDUCTIVITY

An obviously simplified electrical circuit providing semicircles in the complex impedance representation consists of a parallel combination of a pure resistor and a pure capacitor. However, such a representation is oversimplified since the actual (ReZ-ImZ) plots afford semicircles depressed below the real axis. One is then forced to introduce frequency-dependent conductive and/or dielectric properties. Assuming an homogeneous medium, and a linear response of the material to a sinusoidal electric field $E(\omega)$, the total current density J is deduced from Maxwell's equations

$$J=[\sigma(\omega)+j\epsilon_0\epsilon(\omega)\omega]E\ , \tag{1}$$

where j is the square root of -1. Both functions $\sigma(\omega)$ and $\epsilon(\omega)$ obey Kramers-Kronig relations,[12] and as a consequence their real and imaginary parts are not independent. A total conductivity σ_T, $J=\sigma_T$, E, and the admittance Y of the sample are easily derived from Eq. (1):

$$\sigma_T(\omega)=Y(\omega)/L=\sigma(\omega)+j\epsilon_0\epsilon(\omega)\omega\ . \tag{2}$$

At zero frequency, the total conductivity σ_T reduces to the dc conductivity σ_0. Substracting this contribution, a generalized dielectric function

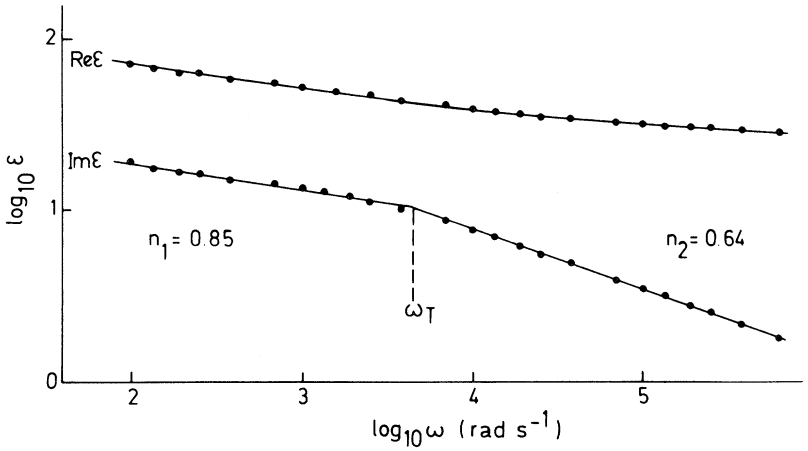

FIG. 4. Plot of the real and imaginary parts of the dielectric response $\epsilon_T(\omega)$ at a given temperature ($T=485$ K), as a function of frequency in a logarithmic system of coordinates. Below and above the transition frequency ω_T, $\mathrm{Im}\epsilon_T$ follows a power-law dependence with different exponents, respectively, equal to (n_1-1) and (n_2-1). Below ω_T both curves are parallel straight lines distant from $\log_{10}[\tan(n_1\pi/2)]$ as expected from Kramers-Kronig relations.

$\epsilon_T(\omega)$ is now defined as

$$\epsilon_T(\omega)=(\sigma_T-\sigma_0)/(j\epsilon_0\omega)\ . \tag{3}$$

Typical variations of the real and imaginary parts of $\epsilon_T(\omega)$ versus frequency are depicted in Fig. 4. Focusing on the imaginary part suggests that the frequency range investigated may be subdivided into two domains, below and above a "transition frequency" ω_T, where a power-law dependence is observed,

$$\mathrm{Im}\epsilon_T(\omega)\propto\omega^{n-1} \tag{4}$$

but with different exponents, respectively, $n_1=0.85$ and $n_2=0.64$, which are found to be temperature independent within experimental uncertainty. As it is done in Appendix A, the frequency dependence of $\mathrm{Re}\epsilon_T$ may be deduced from that of $\mathrm{Im}\epsilon_T$ using the Kramers-Kronig relations.

Above ω_T, the modification brought about by a different frequency behavior at low frequencies decreases as ω^{-2} and is rapidly negligible. As a matter of fact $\mathrm{Re}\epsilon_T$ is not very different from ϵ_∞, the high-frequency dielectric constant.

Below ω_T, the correction arising from the high-frequency behavior is now frequency independent and cancels almost exactly the dielectric constant ϵ_∞. The Kramers-Kronig relations require that $\mathrm{Re}\epsilon_T$ should be proportional to $\mathrm{Im}\epsilon_T$ by a factor of $\tan(n_1\pi/2)$.[12] Indeed, in a logarithmic system of coordinates as in Fig. 4, the two curves are parallel straight lines separated by $\log_{10}[\tan(n_1\pi/2)]$ and ϵ_T may be simply written

$$\epsilon_T(\omega)=C(j\omega)^{n_1-1}\ , \tag{5}$$

where C is a constant. In the complex admittance plane (ReY-ImY), Eqs. (3) and (5) define a straight line of slope $\tan(n_1\pi/2)$. The geometrical inverse in the complex impedance representation is nothing but a circle going through the origin and depressed below the real axis by an angle α, an experimental fact already mentioned in the previous paragraph,

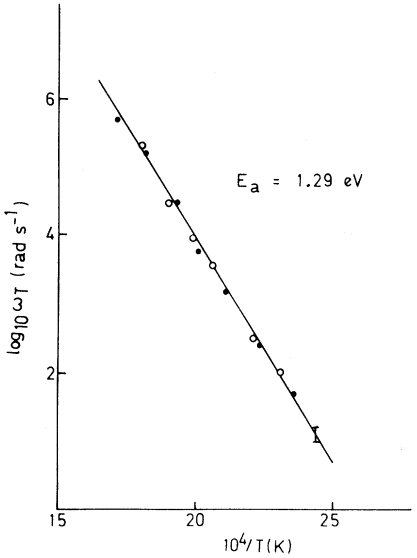

FIG. 5. Plot of the transition frequency ω_T as a function of temperature for two different samples (same symbols as in Fig. 1). Lower right-hand side of the figure indicates (I) the average uncertainty associated with the determination of ω_T. In the temperature range investigated (400–600 K), the mean activation energy ($E_a=1.29$ eV) is equal to that of the electrical conductivity.

$$\alpha=(1-n_1)\pi/2 \ . \tag{6}$$

It must be emphasized that observed depressed circles in the impedance plane are indeed characteristic of the low-frequency region. Above ω_T, because $\mathrm{Re}\epsilon_T$ differs very little from ϵ_∞, the experimental curve shows some parabolic curvature towards the real axis and becomes tangent to the imaginary axis at the highest frequencies.

V. TRANSITION FREQUENCY

The transition frequency ω_T varies with temperature and is thermally activated (Fig. 5). Within the limited temperature interval corresponding to the frequency range investigated ($1-10^5$ Hz), the activation energy appears to be constant and equal to that of the electrical conductivity itself. This strongly suggests that ω_T could be simply related to the jump frequency of the charge carriers in the material. Stabilized zirconia quenched from high temperature possesses a cubic structure of the fluorite type.[8] Heterovalent yttrium ions substitute zirconiums, and charge balance is maintained through the formation of oxygen vacancies, the concentration of which is related to the amount of dopant. Using the Kröger-Vink notation,[13] this process is described by the pseudochemical reaction

$$Y_2O_3 \rightarrow 2Y'_{Zr}+V_O^{\cdot\cdot}+3O_O^X \ . \tag{7}$$

The vacancies are known to be very mobile and responsible for the fast ionic transport of oxygen in such compounds.[1] The electrical conductivity σ_0 may be expressed in terms of the self-diffusion coefficient D_0 through the Nernst-Einstein relationship

$$\sigma_0=D_0Nq^2/k_BT \ , \tag{8}$$

where N and q denote the concentration and the charge of the carriers, respectively, and k_B is the Boltzmann constant. If jumps are assumed to be random and independent of each other, D_0 is simply related to the mean square displacement $\langle r^2\rangle_{\mathrm{av}}$ and the mean residence time $\bar{t}$:

$$D_0=\langle r^2\rangle_{\mathrm{av}}/6\bar{t} \ , \tag{9}$$

$$\langle r^2\rangle_{\mathrm{av}}=\sum_s s^2p_s \ , \tag{10}$$

where p_s denotes the probability of a jump distance

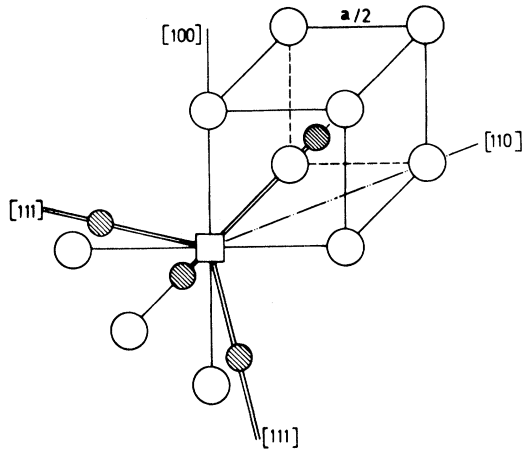

FIG. 6. Part of the fluorite structure around an oxygen vacancy: □, oxygen vacancy; ○, normal oxygen ions; ●, cations.

s ($\sum_s p_s=1$). Combination of Eqs. (8) and (9) yields

$$\nu_T\bar{t}=\frac{Nq^2}{12\pi k_B}\frac{\omega_T}{\sigma_0 T}\langle r^2\rangle_{\mathrm{av}} \ , \tag{11}$$

where ν_T (ω_T) is the transition frequency expressed in Hz (rad s^{-1}). In stabilized zirconia, jumps of the oxygen vacancies take place on the cubic oxygen sublattice, depicted in Fig. 6, the parameter of which is $a/2$. Only jumps to nearest- and next-nearest-neighboring sites need to be considered, respectively, along [100] and [110] directions:

$$\langle r^2\rangle_{\mathrm{av}}=\frac{a^2}{4}(1+p_{110}), \quad 0\le p_{110}\le 1 \ . \tag{12}$$

Using Eqs. (11) and (12), the product $\nu_T\bar{t}$ can be evaluated numerically with an uncertainty of about 10% and varies according to p_{110} between 0.6 ($p_{110}=0$) and 1.1 ($p_{110}=1$). Indeed, ν_T does not appear to be very different from $1/\bar{t}$. However, it must be noticed that in Eq. (9), D_0 is proportional to $1/\bar{t}$, where $\bar{t}$ is the mean residence time, and not to the mean jump frequency. If a statistical distribution of jump frequencies is considered, as will be done in the next sections, both quantities are not *a priori* identical and it is therefore expected that the transition occurs at a frequency different from $1/\bar{t}$.

VI. THEORETICAL APPROACH

As implied by Eq. (2), the measured total conductivity is the sum of two contributions, a con-

ductive σ and a dielectric one ϵ, both of which can be frequency dependent. In an ionically conductive material, the latter arises when localized opposite charges such as (V_O^2, Y'_{Zr}), equivalent to electric dipoles, are present. The imaginary part of $\epsilon(\omega)$ usually fits a broad peak and its variation with frequency is interpreted as due to a distribution of relaxation times.[14] In this study no maximum of $\mathrm{Im}\epsilon_T$ is observed (see Fig. 4) and therefore this model is not applicable to our experimental results. According to Jonscher,[15] a power-law behavior with a change of the exponent at some definite frequency, as reported in Sec. IV, reflects many-body interactions between dipoles. On going from low to high frequencies, an increase of the exponent n is predicted[16] contrarily to the present observations.

Turning now to the conductive contribution, a frequency-dependent conductivity is the consequence of correlated particle jumps.[17] In cubic stabilized zirconia, yttrium ions are randomly distributed and much less mobile than the oxygen vacancies.[1] The electrical interactions between the rigid yttrium network and mobile oxygen vacancies make hops between oxygen sites energetically inequivalent and could be responsible for the correlations.

A general theory of charge transport in disordered systems has been developed by Scher and Lax.[7] Based upon a generalized theory of mobility, it is applicable to any hopping conductive process either ionic or electronic in nature. The motion of carriers is modeled as a continuous-time random walk (CTRW) on a lattice.[18] It is valid over a large frequency range; in particular, Eq. (9) is recovered in the zero-frequency limit. It is also simple since all the disorder is assumed to be included in a single-site waiting-time distribution function $Q(t)$, which is the probability that an oxygen vacancy remains on its site from time $t=0$ until time t. In the original paper of Scher and Lax,[7] $\sigma(\omega)$ is expressed as a function of $\tilde{\psi}(\omega)$, the inverse Fourier transform of which is simply related to $Q(t)$:

$$\mathcal{F}^{-1}(\tilde{\psi})=\psi(t)=\frac{-dQ}{dt} , \tag{13}$$

$$\sigma(\omega)=(Nq^2/k_BT)D(\omega) , \tag{14}$$

$$D(\omega)=\tfrac{1}{6}\langle r^2\rangle_{\mathrm{av}} j\omega\tilde{\psi}(\omega)/[1-\tilde{\psi}(\omega)] . \tag{15}$$

$\psi(t)dt$ represents the probability the time between jumps occurs in the time interval $(t,t+dt)$. On taking the dc limit ($\omega\rightarrow 0$) in Eq. (15), Eq. (9) is obtained with

$$\bar{t}=\int_0^\infty t\psi(t)dt . \tag{16}$$

If $\bar{t}$ is known, the measurement of $\sigma(\omega)$ as a function of frequency allows the calculation of $\tilde{\psi}(\omega)$ or equivalently of $\tilde{Q}(\omega)$, the Fourier transform of $Q(t)$:

$$\tilde{\psi}(\omega)=1-j\omega\tilde{Q}(\omega) , \tag{17}$$

$$\tilde{Q}(\omega)/\bar{t}=(\sigma/\sigma_0+j\omega\bar{t})^{-1} . \tag{18}$$

When the conductivity $\sigma(\omega)$ is frequency independent, the function $\tilde{Q}(\omega)/\bar{t}$ reduces to a single relaxation time, i.e., the imaginary part is a Lorentzian curve centered on $\omega=1/\bar{t}$. A frequency-dependent conductivity broadens and displaces this distribution. From the quantitative treatment presented in Sec. VII, it can be assumed that the imaginary part is indeed centered on ν_T, the transition frequency.

A microscopic model is now needed in order to account for the probability function $Q(t)$ thereby obtained. Let us consider a vacancy on an oxygen site labeled $i0$ and $Q_{i0}(t)$ as the probability that the carrier remains on its site at a time t. This probability decreases in time, via all the n parallel decay channels by which it can transfer to a neighboring site, for instance, along the six [100] directions,

$$\frac{dQ_{i0}(t)}{dt}=-Q_{i0}(t)\sum_{j=1}^{n} W(r_j) , \tag{19}$$

where $W(r_j)$ is the transition rate between neighboring sites in the jth direction. Taking into account the fact that $Q_{i0}(0)=1$, Eq. (19) can be integrated:

$$Q_{i0}(t)=\prod_{j=1}^{n}\exp[-W(r_j)t] . \tag{20}$$

The probability $Q(t)$ is obtained as the configuration average of $Q_{i0}(t)$. In a cubic lattice, the n jump directions are equivalent and statistically independent. Therefore,

$$Q(t)=q^n(t) \tag{21}$$

with

$$q(t)=\int_0^\infty dW f(W)\exp(-Wt), \quad t\geq 0 \tag{22}$$

where $f(W)$ is the transition-rate distribution function associated with one jump direction. Mathematically, $q(t)$ is the Laplace transform of $f(W)$ and because of the convolution theorem,[12] $Q(t)$ is the Laplace transform of $F(W)$, the n-fold self-convolution of $f(W)$:

$$F(W)=f(W)^{*n} \tag{23}$$

$$Q(t)=\int_0^\infty dW\,F(W)\exp(-Wt)\ . \tag{24}$$

The Fourier transform $\tilde{Q}(\omega)$ is related to $F(W)$ through a Stieltjes transform:

$$\tilde{Q}(\omega)=\int_0^\infty dW\frac{F(W)}{W+j\omega}\ , \tag{25}$$

or equivalently, using $\tau=1/W$ as the integration variable

$$\tilde{Q}(\omega)/\bar{t}=\int_{\tau=0}^\infty \frac{G(\ln\tau)}{1+j\omega\tau}d(\ln\tau) \tag{26}$$

with

$$F(W)=\bar{t}G(-\ln W)\ . \tag{27}$$

Several methods exist to obtain information concerning the distribution function $G(\ln\tau)$, a survey of which can be found in Ref. 12.

To summarize, the motion of the oxygen vacancies has been modeled as a continuous-time random walk on a simple cubic lattice. The transition rate is treated as a random variable the distribution function of which is $f(W)$. All the dynamics of the motion is incorporated into $Q(t)$ which is related to $f(W)$ through several mathematical steps, e.g., Eqs. (21)—(24), and which can be determined from experimental data. The transition rate W, being temperature activated, is a very sensitive function of the energy barrier

$$W=W_0\exp[-(E/k_BT)] \tag{28}$$

and a distribution of energy barriers $g(E)$ can be deduced from $f(W)$ according to

$$g(E)=f(W)\frac{dW}{dE}\ . \tag{29}$$

VII. DETERMINATION OF $G(\ln\tau)$

Before proceeding any further, let us emphasize that only the total conductivity $\sigma_T(\omega)$ is measured. As a conclusion of the above discussion in Sec. VI, it will be hypothesized that the frequency-dependent dielectric contribution is negligible compared to that of the electrical conductivity $\sigma(\omega)$. Then Eq. (2) writes

$$\sigma_T(\omega)\simeq\sigma(\omega)+j\epsilon_0\epsilon_\infty\omega\ , \tag{30}$$

where ϵ_∞, experimentally known, is the high-frequency dielectric constant associated with atomic and electronic polarizations. In order to com-

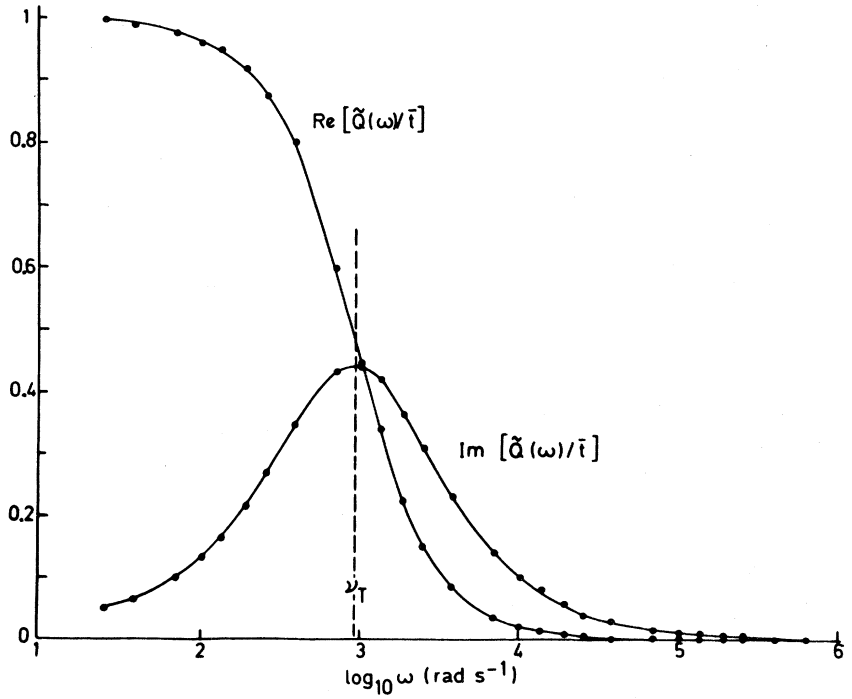

FIG. 7. Plot of the real and imaginary part of $\tilde{Q}(\omega)/\bar{t}$ at a given temperature ($T=495$ K) as a function of frequency. Numerical values have been derived from ac electrical conductivity measurements using Eqs. (18) and (30). Parameter $\bar{t}$ has been chosen in such a way that the maximum of the imaginary part of $\tilde{Q}(\omega)/\bar{t}$ occurs at $\omega=\nu_T$.

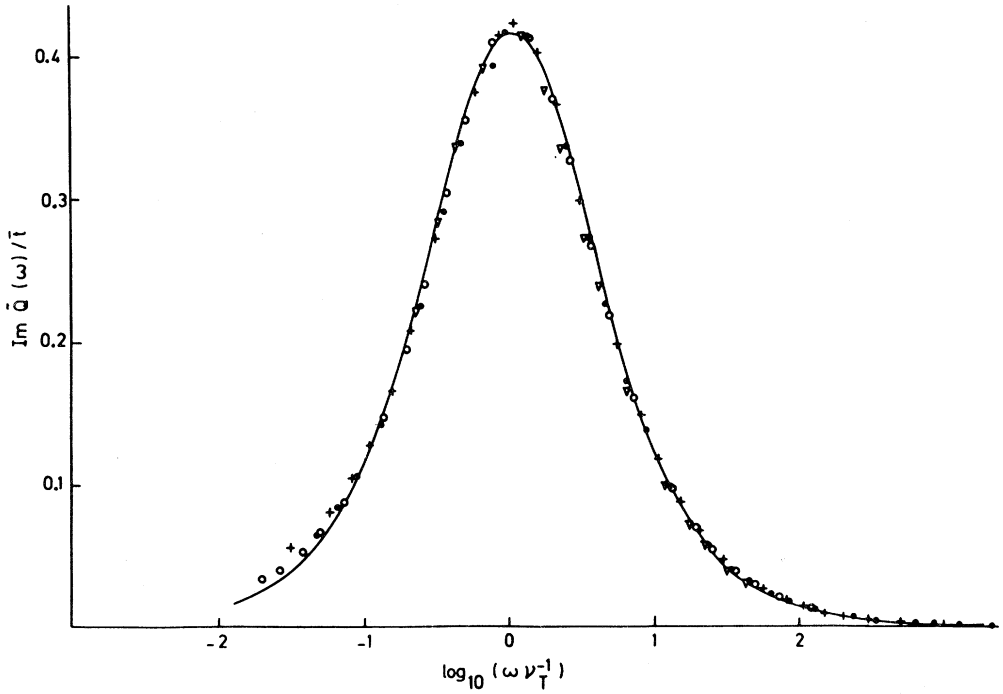

FIG. 8. Plot of the imaginary part of $\tilde{Q}(\omega)/\bar{t}$ as a function of frequency at different temperatures (∇, 449 K; ●, 473 K; +, 495 K; ○, 519 K). Frequency scale has been normalized to ν_T the transition frequency, and, as a consequence, a unique curve is defined which corresponds to a Wagner-Yager distribution of the jump frequencies (full curve).

pute $\tilde{Q}(\omega)/\bar{t}$ using Eqs. (30) and (18), the mean residence time $\bar{t}$ or, equivalently, the mean-square displacement $\langle r^2\rangle_{\text{av}}$ is needed. As mentioned in Sec. V, the latter can be varied between one and twice $a^2/4$, respectively, the shortest and next shortest jump distance. In any case, the calculated imaginary part of $\tilde{Q}(\omega)/\bar{t}$ is a bell-shaped curve while the real part of $\tilde{Q}(\omega)/\bar{t}$ goes from zero to one with decreasing frequency as presented in Fig. 7. In the case of a frequency-independent conductivity $\sigma(\omega)$, $\text{Im}\tilde{Q}(\omega)/\bar{t}$ is a Lorentzian curve centered on $\omega(\text{rad s}^{-1})=1/\bar{t}$ (s). The consequence of a dispersive $\sigma(\omega)$ is that the abscissa of the maximum no longer coincides with $1/\bar{t}$. Indeed it is found that for $\langle r^2\rangle_{\text{av}}=1.4a^2/4$, the maximum occurs at ν_T, the transition frequency. According to Eq. (12), this would imply that 40% of the jumps occur along [110] and 60% along [100]. In fact, taking the large uncertainty associated with the determination of ν_T into account, it would be safer to say that the probability of the [100] jump direction is in the (50—70 %) range. The diffusive motion of the fluorine ions in CaF_2, a compound very similar to yttria-stabilized zirconia, has been simulated with the method of molecular dynamics.[19] Jumps are found to occur mainly along [100] with a probability of 80% in agreement with our assumption. Because ν_T is activated with the same activation energy as the electrical conductivity, the calculated data of $\text{Im}\tilde{Q}(\omega)/\bar{t}$ at different temperatures give a unique curve, reported on Fig. 8, when plotted as a function of $\omega\nu_T^{-1}$.

The study of the distribution of relaxation times $G(\ln\tau)$ associated with $\tilde{Q}(\omega)/\bar{t}$, Eq. (26), is made easier using the so-called Cole-Cole plot,[12] obtained by graphing the imaginary part versus the real part of $\tilde{Q}(\omega)/\bar{t}$ in the complex plane and depicted in Fig. 9. Then distinct features appear immediately. First, the Cole-Cole plot is symmetrical with respect to the maximum and so will be the distribution $G(\ln\tau)$. Second, it intersects the real axis at the high- and low-frequency sides under right angles. These two properties are verified by the Wagner-Yager distribution introduced into the theory of dielectric relaxation in 1913 by Wagner[20]:

$$G(\ln\tau)=\frac{1}{B\sqrt{2\pi}}\exp[-(\ln\Omega_0\tau)^2/2B^2]\ , \qquad (31)$$

where Ω_0 coincides with the maximum of the bell-shaped curve, i.e., $\Omega_0=\nu_T$, and B is a constant. The integral, Eq. (26), can only be evaluated in closed form for special cases, i.e., for $\text{Im}\tilde{Q}(\omega)/\bar{t}$ when $2\ln(\omega/\Omega_0)/B^2$ is an odd integer and for $\text{Re}\tilde{Q}(\omega)/\bar{t}$ when it is an even integer. Otherwise, it

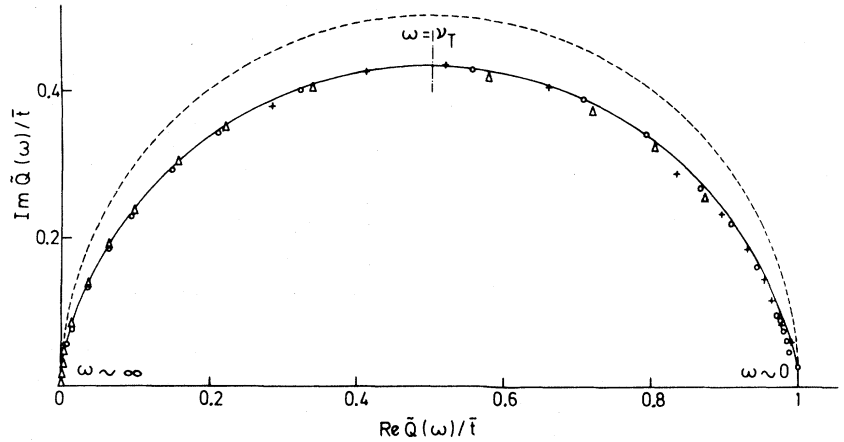

FIG. 9. Cole-Cole plot ($\mathrm{Re}\tilde{Q}(\omega)/\bar{t}$-$\mathrm{Im}\tilde{Q}(\omega)/\bar{t}$) is used for the determination of the distribution function associated with $\tilde{Q}(\omega)/\bar{t}$. It must be noticed that the graph is symmetrical with respect to $\omega=\nu_T$ and intersects the real axis at right angles. For comparison two curves are given; the first one is associated with a single-frequency distribution function (dotted line), the second one with a Wagner-Yager distribution (full curve).

has to be evaluated numerically using a computer program. Very good agreement with the experimental data is obtained after putting $B^2=0.5$ in Eq. (31), as shown in Fig. 8. The function $Q(t)$ fulfills two conditions and so does the distribution $G(\ln\tau)$:

$$\bar{t}=\int_0^\infty Q(t)dt=\int_0^\infty t\psi(t)dt\ , \tag{32}$$

$$1=Q(0)=\int_0^\infty \psi(t)dt\ . \tag{33}$$

Using Eqs. (26) and (31), the first condition, Eq. (32), appears to be always verified. The second condition, Eq. (33), imposes some relation between $\bar{t}$ and ν_T:

$$\nu_T\bar{t}\exp(B^2/2)=1\ . \tag{34}$$

The left-hand side of Eq. (34), in which all parameters are independently known, is indeed found to be equal to 0.9 ± 0.2.

VIII. MICROSCOPIC INTERPRETATION

In the proposed microscopic model, oxygen vacancies jump over energy barriers which are nonuniform in the material. More precisely variations in the heights of the barriers are produced through interactions between the charge carriers and the immobile yttrium ions which are randomly distributed in the sample. From Eqs. (23) and (29), the statistical distribution of the jump frequencies $f(W)$ and ultimately of the activation energies $g(E)$ can be, in principle, determined. Unfortunately, two different distributions $f(W)$ have to be associated with the two jump directions which have been considered, while only one total jump-frequency distribution $F(W)$ is experimentally known. This led us to consider only one jump direction, namely [100], which appears to be the most probable one, an approximation which will be discussed later on.

According to Eq. (23), $f(W)$ is related to $F(W)$ through an n-fold self-convolution where n is the coordination number of the oxygen vacancy, i.e., $n=6$ within the above approximation. Deconvolution is a difficult mathematical problem and no exact analytical solution exists in the specific case of a Wagner-Yager distribution. Nevertheless, as shown in Appendix B, the convolution of a Wagner-Yager distribution by itself, computed numerically, is well approximated by Wagner-Yager distribution. Therefore the two parameters ω_0 and b can be deduced from two general properties of the convolution product; the average value and the mean-square deviation of an n-fold self-convolution of $f(W)$ are n times the average value and the mean-square deviation of $f(W)$.[21] Taking the fact that $f(W)$ is normalized to unity into account, these relations become

$$\exp b^2=1+n(\exp B^2-1)\ , \tag{35}$$

$$\Omega_0/\omega_0=n\exp[-\tfrac{3}{2}(B^2-b^2)]\ , \tag{36}$$

where b and ω_0 (respectively, B and Ω_0) characterize $f(W)$ [respectively, $F(W)$]. With $B^2=0.5$ (cf. Sec. VII), b^2 and Ω_0/ω_0 calculated through Eqs. (35) and (36) are, respectively, equal to 1.59 and 30.7.

Then a distribution of the barrier heights can be

deduced using Eqs. (28) and (29). After some lengthy manipulations $g(E)$ is found to be

$$g(E)=\frac{1}{bk_BT\sqrt{2\pi}}\exp\left[-\frac{(E-\bar{E})^2}{2(bk_BT)^2}\right]. \quad (37)$$

This a Gaussian distribution, centered on $\bar{E}$ the mean-square deviation of which is bk_BT. The centroid $\bar{E}$ is equal to

$$\bar{E}=E_a-k_BTb^2, \quad (38)$$

where E_a is the activation energy of ω_0 (or equivalently of $\Omega_0=\nu_T$) and of the electrical conductivity, i.e., $E_a=1.29$ eV. The correction term b^2k_BT is quantitatively very small, of the order of 5%. The width to half-peak of the distribution is equal to $2.36k_BT$, i.e., 0.13 eV in the temperature range investigated, a reasonable value when compared to the largest interaction energy between an oxygen vacancy and a yttrium ion, i.e., 0.43 eV.[22]

Returning to Eq. (35) it may be seen that for large values of n, b^2 depends logarithmically on n, the coordination number. Therefore, if the [110] jump direction is now considered instead of [100], with $n=12$, the width of the Gaussian distribution changes only from 0.13 to 0.15 eV. This insures that the approximation which has been used throughout this paragraph is not too drastic.

IX. SUMMARY

Both electric and dielectric properties of yttria-stabilized zirconia, known to be a good anionic conductor at high temperature have been studied as a function of frequency ($1-10^5$ Hz) and temperature (400–1100 K). The precise measurement of the dc electrical conductivity, especially at the lowest temperature, was made possible using the complex impedance representation.[6] It is found to be temperature activated, the activation energy changing gradually from 1.33 to 1.17 eV when going from low to high temperature. As a function of frequency, the electrical conductivity exhibits a power-law dependence with a different exponent n at low ($n=0.85$) and at high frequencies ($n=0.64$). On a logarithmic scale, the transition occurs at a definite frequency ω_T, activated with the same activation energy as the electrical conductivity. According to linear response theory developed by Kubo,[23] a frequency-dependent conductivity results from correlations between charge carriers. These are oxygen vacancies, with a positive +2 formal charge with respect to the ideal defectless lattice, which compensate charge deficiency of heterovalent yttrium ions. It is thought that electrical interactions between the mobile charges and the immobile and randomly distributed yttrium ions make jumps of the charge carriers energetically nonequivalent and are responsible for the correlations. Using the theory of stochastic transport in disordered systems elaborated by Scher and Lax,[7] a statistical distribution of the jump frequencies is determined, found to be a Wagner-Yager distribution, the maximum of which coincides with ν_T, the transition frequency. This implies a Gaussian distribution of the energy barrier heights which the charge carriers have to jump over, centered on the activation energy E_a of the electrical conductivity and with a width to half-peak of 0.13 eV. This interpretation has been experimentally established only in the (400–600 K) temperature range when jump frequencies fall into the accessible frequency range ($1-10^5$ Hz). Ultimately it must be noticed that, using the same description, computer simulation has been able to reproduce the remarkable qualitative features of the conductivity measurements on the anion deficient fluorite oxides, that is the decrease in electrical conductivity with increasing dopant concentration.[5]

A power-law frequency dependence $\sigma(\omega)\propto\omega^n$ has often been found in electronically conducting materials such as impurity-doped semiconductors,[24] scandium oxide thin films,[25] or glasses.[26] Current work[27] in our laboratory on glasses shows that similar results are obtained for different ionically conducting materials, at least when dielectric losses associated with localized charge motions are negligible. Indeed the transport theory developed by Scher and Lax seems general and applies in various cases where independent carriers move from one localized center to another by hopping. As a consequence, the Gaussian distribution of activation energies already proposed to explain ionic conduction in lithium containing glasses[28] could be of a very general character.

APPENDIX A

In the frequency range investigated, the imaginary part of $\epsilon(\omega)$ follows a power-law dependence with different exponents above and below the transition frequency ω_T:

$$\mathrm{Im}\epsilon(\omega)\propto\begin{cases}\omega^{n_1-1}, & \omega\le\omega_T \quad (A1)\\ \omega^{n_2-1}, & \omega\ge\omega_T . \quad (A2)\end{cases}$$

Assuming that this experimental result is valid over the entire frequency range the real part of $\epsilon(\omega)$ may be calculated with the help of the Kramers-Kronig relations[12]

$$\mathrm{Re}\epsilon(\omega)=\epsilon_\infty+\frac{2}{\pi}\int_0^\infty dx\frac{x\,\mathrm{Im}\epsilon(x)}{x^2-\omega^2}\ . \tag{A3}$$

The integral in Eq. (A3) may be evaluated differently for frequencies below and above ω_T as follows.

(a) $\omega \gg \omega_T$:

$$\mathrm{Re}\epsilon(\omega)=\epsilon_\infty+\frac{2}{\pi}\int_0^\infty dx\frac{x\,\mathrm{Im}\epsilon_2}{x^2-\omega^2}+\frac{2}{\pi}\int_0^{\omega_T} dx\frac{x\,\mathrm{Im}(\epsilon_1-\epsilon_2)}{x^2-\omega^2}\ , \tag{A4}$$

where the indices 1 and 2 denote the different analytical forms of the imaginary part of $\epsilon(\omega)$, respectively, below and above ω_T. Therefore, at high frequencies,

$$\mathrm{Re}\epsilon(\omega)\simeq\mathrm{Re}\epsilon_2(\omega)-\frac{2}{\pi}\omega^{-2}\int_0^{\omega_T} dx\,x\,\mathrm{Im}(\epsilon_1-\epsilon_2)\ . \tag{A5}$$

Taking Eqs. (A1) and (A2) into account,

$$\mathrm{Re}\epsilon(\omega)\simeq\mathrm{Re}\epsilon_2(\omega)+\frac{2}{\pi}(\omega_T/\omega)^2\frac{(n_1-n_2)}{(n_1+1)(n_2+1)}\times\mathrm{Im}\epsilon(\omega_T)\ . \tag{A6}$$

The correction to $\mathrm{Re}\epsilon_2(\omega)$ brought about by a different exponent at low frequencies, calculated numerically with $n_1=0.85$, $n_2=0.64$, and $\mathrm{Im}\epsilon(\omega_T)\simeq 10$ is equal to $0.44(\omega_T/\omega)^2$. Compared to $\epsilon_\infty\simeq 28$ this correction is rapidly negligible with increasing frequencies.

(b) $\omega \ll \omega_T$:

$$\mathrm{Re}\epsilon(\omega)=\epsilon_\infty+\frac{2}{\pi}\int_0^\infty dx\frac{x\,\mathrm{Im}\epsilon_1}{x^2-\omega^2}+\frac{2}{\pi}\int_{\omega_T}^\infty dx\frac{x\,\mathrm{Im}(\epsilon_2-\epsilon_1)}{x^2-\omega^2}\ . \tag{A7}$$

At low frequencies

$$\mathrm{Re}\epsilon(\omega)\simeq\mathrm{Re}\epsilon_1(\omega)+\frac{2}{\pi}\int_{\omega_T}^\infty dx\frac{\mathrm{Im}(\epsilon_2-\epsilon_1)}{x}\ . \tag{A8}$$

The correction to $\mathrm{Re}\epsilon_1(\omega)$ is now frequency independent. Negative, it tends to reduce ϵ_∞ from

$$\Delta\epsilon_\infty=\frac{2}{\pi}\frac{(n_1-n_2)}{(1-n_1)(1-n_2)}\mathrm{Im}\epsilon(\omega_T)\ . \tag{A9}$$

Using the same figures as above, this correction is important, $\Delta\epsilon_\infty\simeq 25$ in agreement with experimental data.

APPENDIX B

As mentioned in Sec. VIII, no exact analytical solution of the self-convolution of a Wagner-Yager distribution exists to our knowledge in the literature. Nevertheless, it may be concluded from numerical computation, presented below, that it closely approximates a Wagner-Yager distribution

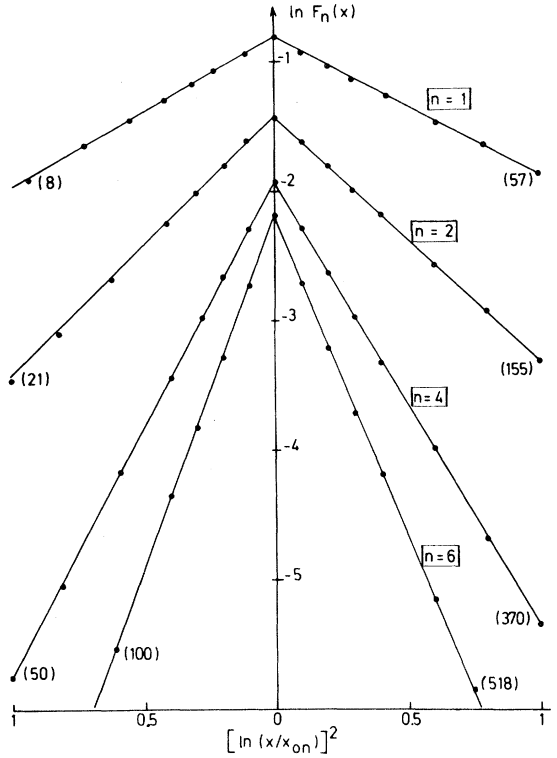

FIG. 10. Using a fast Fourier-transform program, the n-fold self-convolution $F_n(x)$ of $f(x)$, Eq. (B1), has been calculated for different values of n. Numerical results are presented in a $\log_{10}F_n(x)$-$[\log_{10}(x/x_{0n})]^2$ plot where x_{0n} is the abscissa of the maximum, see Table I. Points to the right (respectively, left) of the origin correspond to abscissas (given in parentheses in Δx unit) greater (respectively, smaller) than x_{0n}. Graphs appear to be straight lines of slopes $1/2B_n^2$, symmetrical with respect to the origin.

TABLE I. Comparison between numerically calculated and *a priori* predicted values of the parameters A_n, x_{0n}, and B_n in Eq. (B2), for different n-fold self-convolution of $f(x)$ ($n=1,2,4,6$). (1) Derived from Fig. 10; (2) predicted using Eqs. (36), (37), and (B3); (3) expressed in Δx unit (0.05).

	$x_{0n}(3)$		B_n		A_n	
n	(1)	(2)	(1)	(2)	(1)	(2)
1	21	20	0.47	0.50	0.439	0.439
2	57	55.6	0.27	0.28	0.241	0.236
4	136	135.2	0.147	0.150	0.146	0.141
6	218	217.8	0.103	0.103	0.112	0.110

within numerical uncertainty. It is well known that convolution of two functions means multiplication of their Fourier transforms.[21] This fundamental property has been used to calculate the n-fold self-convolution $F_n(x)$ of the following test function normalized to unity:

$$f(x)=\frac{e^{-1/4}}{\sqrt{\pi}}\exp[-(\ln x)^2] \tag{B1}$$

using a fast Fourier-transform program (Harwell Library, $N=1024$ points, Δx step$=0.05$, double precision numbers). Computed numerical results are presented in Fig. 10 with $\ln F_n(x)$ on the y axis and $[\ln(x/x_{0n})]^2$ on the x axis, where x_{0n} is the abscissa of the maximum. In agreement with what is expected for a Wagner-Yager distribution, a linear relationship is observed. The graph is slightly asymmetrical with respect to x_{0n}, even in the case of n equal to one; this is due to the inherent uncertainty, equal to $\pm\Delta x$, associated with the determination of the maximum. Finally, the computed function $F_n(x)$ may be written

$$F_n(x)=A_n\exp\{[\ln(x/x_{0n})]^2/2B_n^2\}\ , \tag{B2}$$

where the three parameters, x_{0n} abscissa of the maximum, A_n maximum of $F_n(x)$, and $1/2B_n^2$ slope of the straight line (see Fig. 10), are determined numerically. As explained in Sec. VIII, general properties of the convolution product can be used to predict *a priori* the values of x_{0n} and B_n. Likewise, the self-convolution of a normalized function is also normalized and A_n is given by

$$A_n=\frac{\exp[-(B_n^2/2)]}{x_{0n}B_n\sqrt{2\pi}}\ . \tag{B3}$$

Predicted and calculated values of x_{0n}, B_n, and A_n are summarized in Table I. A very good agreement is indeed observed.

[1]T. H. Etsell and S. N. Flengas, Chem. Rev. 70, 339 (1970).

[2]T. H. Etsell and S. N. Flengas, Metall. Trans. 3, 27 (1972).

[3]R. G. Fuller, *Point Defects in Solids,* edited by J. H. Crawford and L. M. Slifkin (Plenum, New York, 1972), Vol. I, p. 103.

[4]H. Schmalzried, Z. Phys. Chem. Neue Folge 105, 47 (1977).

[5]C. R. A. Catlow, *Computer Simulation in the Physics and Chemistry of Solids,* Proceedings of the Daresbury Study Weekend, 1980, edited by C. R. A. Catlow, W. C. Mackrodt, and V. R. Saunders (Science Research Council, Daresbury, Great Britain, 1980).

[6]J. E. Bauerle, J. Phys. Chem. Solids 30, 2657 (1969).

[7]H. Scher and M. Lax, Phys. Rev. B 7, 4491 (1973).

[8]V. I. Aleksandrov, V. V. Osiko, A. M. Prokhorov, and V. M. Tatarintsev, in *Current Topics in Materials Science,* edited by E. Kaldis (North-Holland, Amsterdam, 1978), Vol. I, p. 1.

[9]J. L. Servoin and F. Gervais (unpublished).

[10]E. Schouler, M. Kleitz, and C. Desportes, J. Chim. Phys. (Paris) 70, 1309 (1973).

[11]S. P. S. Badwal and H. J. De Bruin, Phys. Status Solidi A 54, 261 (1979).

[12]C. J. F. Böttcher and P. Bordewijk, *Theory of Electric Polarization* (Elsevier, Amsterdam, 1978), Vol. II, p. 30.

[13]F. A. Kröger, *The Chemistry of Imperfect Crystals,* 2nd ed. (North-Holland, Amsterdam, 1974), Vol. II, p. 1.

[14]W. A. Yager, Physics (continued as J. Appl. Phys.) 7, 434 (1936).

[15]A. K. Jonscher, Phys. Status Solidi A 32, 665 (1975).

[16]K. L. Ngai, A. K. Jonscher, and C. T. White, Nature (London) 277, 185 (1979).

[17]H. R. Zeller, H. U. Beyeler, P. Bruesch, L. Pietronero, and S. Strässler, Electrochim. Acta 24, 793 (1979).

[18]E. W. Montroll and G. H. Weiss, J. Math. Phys. 6, 167 (1965).
[19]G. Jacucci and A. Rahman, J. Chem. Phys. 69, 4117 (1978).
[20]K. W. Wagner, Ann. Phys. (Leipzig) 40, 817 (1913).
[21]R. Bracewell, *The Fourier Transform and Its Applications* (McGraw-Hill, New York, 1965).
[22]Interaction energy calculated on the basis of purely electrostatic interaction in a dielectric medium ($\epsilon_\infty \simeq 25$) between an oxygen vacancy (effective charge $+2$) and an yttrium ion (effective charge -1) as nearest-neighbor sites (see Fig. 6: $r = a\sqrt{3}/4$).
[23]R. Kubo, *Tokyo Summer Lectures in Theoretical Physics, Part I: Many-body Theory* (Benjamin, New York, 1965).
[24]M. Pollak and T. H. Geballe, Phys. Rev. 122, 1742 (1961).
[25]G. E. Pike, Phys. Rev. B 6, 1572 (1972).
[26]D. Ravaine, J. P. Diard, and J. L. Souquet, Trans. Faraday Soc. 71, 1935 (1975).
[27]P. Abelard and J. F. Baumard (unpublished).
[28]A. M. Glass and K. Nassau, J. Appl. Phys. 51, 3756 (1980).